

Three-dimensional textures and defects of soft material layering revealed by thermal sublimation

Dong Ki Yoon^{a,b,1,2}, Yun Ho Kim^{c,1}, Dae Seok Kim^a, Seong Dae Oh^a, Ivan I. Smalyukh^{b,d}, Noel A. Clark^{b,2}, and Hee-Tae Jung^{e,2}

^aGraduate School of Nanoscience and Technology and KINC, and ^eNational Research Laboratory for Organic Opto-Electronic Materials, Department of Chemical and Biomolecular Engineering, Korea Advanced Institute of Science and Technology, Daejeon 305-701, Korea; ^bDepartment of Physics and Liquid Crystal Materials Research Center, and ^dRenewable and Sustainable Energy Institute, University of Colorado, Boulder, CO 80309; and ^cAdvanced Functional Materials Research Group, Korea Research Institute of Chemical Technology, Daejeon 305-600, Korea

Contributed by Noel A. Clark, October 15, 2013 (sent for review August 28, 2013)

Layering is found and exploited in a variety of soft material systems, ranging from complex macromolecular self-assemblies to block copolymer and small-molecule liquid crystals. Because the control of layer structure is required for applications and characterization, and because defects reveal key features of the symmetries of layered phases, a variety of techniques have been developed for the study of soft-layer structure and defects, including X-ray diffraction and visualization using optical transmission and fluorescence confocal polarizing microscopy, atomic force microscopy, and SEM and transmission electron microscopy, including freeze-fracture transmission electron microscopy. Here, it is shown that thermal sublimation can be usefully combined with such techniques to enable visualization of the 3D structure of soft materials. Sequential sublimation removes material in a stepwise fashion, leaving a remnant layer structure largely unchanged and viewable using SEM, as demonstrated here using a lamellar smectic liquid crystal.

sublime | direct visualization

The study of the structure of layered soft materials began in the early 1900s with the legendary inference of Grandjean and Friedel of the fluid layer structure of smectic liquid crystals (LCs) based on their observation of the elliptical core lines of focal conic defects and their interpretation of these as the singularities that appear when space is filled with equally spaced curved surfaces generated from the cyclides of Dupin (1–4). Since that time, the techniques of X-ray diffraction, and visualization, using optical transmission and fluorescence confocal polarizing microscopy; atomic force microscopy (AFM); and SEM and transmission electron microscopy (TEM), including freeze fracture TEM (FFTEM), have been widely applied to characterize soft layering and defects (5–10), but the ability to visualize layering directly throughout a 3D sample (e.g., in particular confinement conditions) has been limited. Here, we apply thermal sublimation, a technique that is widely applicable due to the relatively low vapor pressure of many soft material components, as a method for removing material from a 3D sample that maintains its internal structure (i.e., moves the material surface into the bulk, creating a deeper interface that exhibits a topography that reflects the local structure).

We demonstrate this method using the thermal sublimation of a fluid smectic LC phase, wherein the LC material was removed layer by layer. We show that even in small-molecule, high-temperature fluid smectic A (SmA) phases, the underlying layer structure successfully resists surface tension (which tends to smooth out the advancing interface) to yield a surface topography that exhibits features of the underlying layer structure. Local features, such as defects, can advance or retard sublimation, leading to distinct visualization and control effects. The full 3D structure of a layered sample was exposed by successive sublimation steps and maintained during visualization by cooling. The remnant structure was observed under polarized light microscopy

(PLM) as an evolution of the optical texture, and with suboptical resolution using EM and AFM techniques to probe the remnant interface topographic structure. Experiments reported here show that sublimation is useful for visualizing 3D layering and should be broadly applicable to the study of soft matter structure when combined with available fixing and visualization methods (11–15).

Results

Thermal Sublimation of Soft Layers. We study the molecule YHK1 (13, 16), which orders at high temperature into a SmA phase with its characteristic fluid-layered focal conic defects and textures, and then retains this layer structure as it is cooled to room temperature into a soft crystal phase. Upon cooling, the semi-fluorinated rod-like molecule YHK1 showed thermal transitions from the isotropic phase to a SmA-like phase, and then to the more ordered SmX₁ and soft crystal phases (17). X-ray diffraction of an oriented domain (*SI Appendix, Fig. S1*) shows the SmA and SmX₁ phases to be locally polar ordered, but with a modulation of the sign of the polar ordering parallel to the layer planes (i.e., a SmA phase that has body-centered rectangular domains) (18, 19). At small angles, this produces a lattice of peaks indexing to a centered rectangular layer/modulation lattice. With cooling, additional peaks appear at high angles, indicating the development of in-plane positional order, but the modulation lattice persists with very little change in structure or lattice parameters down into the soft crystal phase at room temperature. The SmA-SmX₁ and SmX₁-crystal (Cr) transitions appear continuous in X-ray scattering and show a continuous evolution in PLM optical textures. Thus, the layer structure adopted by YHK1 in the SmA phase persists upon cooling down to room temperature, gradually

Significance

Techniques that enable direct visualization in three dimensions of internal nanometer- to micrometer-scale structure are highly prized in materials research and engineering. Here, we demonstrate an effective method for the 3D imaging of soft materials, revealing the alignment, textures, and defects in the organization of their internal interfaces: in this case, of a soft crystal and liquid crystal phase. This method employs combinations of quenching and sublimation generating surface topography that reflects the internal structure, exposing it for visualization using standard techniques.

Author contributions: D.K.Y. and H.-T.J. designed research; D.K.Y. and Y.H.K. performed research; D.K.Y., Y.H.K., D.S.K., S.D.O., I.I.S., and N.A.C. contributed new reagents/analytic tools; D.K.Y., Y.H.K., D.S.K., I.I.S., N.A.C., and H.-T.J. analyzed data; and D.K.Y., Y.H.K., I.I.S., N.A.C., and H.-T.J. wrote the paper.

The authors declare no conflict of interest.

¹D.K.Y. and Y.H.K. contributed equally to this work.

²To whom correspondence may be addressed. E-mail: nandk@kaist.ac.kr, noel.clark@colorado.edu, or heetae@kaist.ac.kr.

This article contains supporting information online at www.pnas.org/lookup/suppl/doi:10.1073/pnas.1317922110/-DCSupplemental.

becoming more solid-like and thus freezing in the SmA layer texture. YHK1 therefore has structural characteristics convenient for thermal sublimation studies of smectic layer organization.

Sample drops were spread to a 5- to 10- μm thickness in the isotropic phase on glass or silicon wafer surfaces previously spin-coated with polyethyleneimine (PEI; Aldrich; molecular weight of 60,000) to provide random planar anchoring of the LC. Upon cooling into the SmA, the surface thus induces planar alignment, whereas the top of the LC film was open to air to induce homeotropic alignment. The resulting geometrical frustration can be accommodated by the formation of toroidal focal conic domains (TFCDs) (12, 13, 20, 21). In the thin films prepared here, this tendency led to the spontaneous appearance of large hexagonal arrays of uniformly sized and spaced TFCDs, shown in PLM in Fig. 1B and SI Appendix, Fig. S2, obtained by holding the sample temperature $\sim 5^\circ\text{C}$ below the Iso-SmA transition temperature for a few minutes. These circular birefringent domains have the classic TFCDs, extensively characterized in previous research, within which the smectic layers form a set of nested

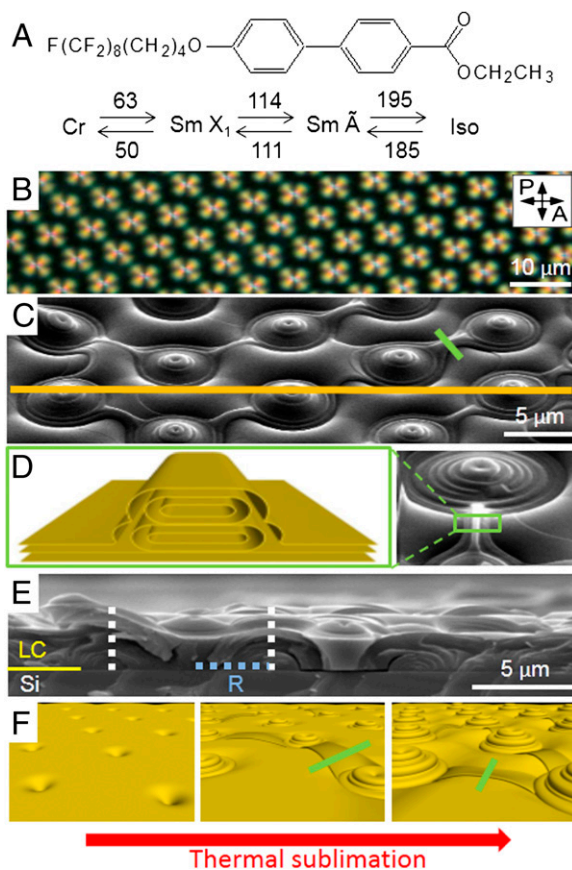


Fig. 1. LC material and the surface- and internal structure of thermally sublimated TFCDs. (A) Molecular structure, phases, and transition temperatures ($^\circ\text{C}$) of the rod-like smectic LC material, YHK1. (B) PLM texture shows hexagonally arranged TFCDs and a typical Maltese-cross pattern of each TFCD. A, analyzer; P, polarizer. (C) SEM image shows dome structures with concentric rings that look isolated from each other in thin film. (D) Schematic illustration of connected smectic layers between cones of TFCDs (green lines in C and F) shows how multi-Burgers vector edge dislocations are formed. (E) Direct view of internal structure of fractured dome morphologies by SEM shows that this unique morphology is based on a normal TFCD; the height of the interconnect area is lower than that of dimples of TFCDs. White lines represent a wall of imaginary cylinders of TFCDs; the blue line is the radius (R) of those. (F) Schematic illustrations present dome structure development from normal TFCDs during the thermal sublimation process.

toroidal surfaces bounded by a cylinder normal to the surface with layer cusps along a straight line passing through the axis of the cylinder (1, 22) (SI Appendix, Fig. S2). The known layer structures of these TFCD arrays make them attractive candidates for the evaluation of thermal sublimation as a probe of smectic layer structure.

Sublimation studies were done on these YHK1 films by first cooling the films to room temperature and assessing them optically for the desired annealed textures. Sublimation was then carried out by successive steps of heating into the SmA phase [to a temperature (T) of $\sim 180^\circ\text{C}$] for ~ 2 min and then cooling back to room temperature. Each such step removed some LC material from the surface of the film by sublimation. The resulting surface topography was visualized by sputter-coating platinum (Pt) film on the room temperature LC surface and imaging it using SEM. Images of the cross-sectional topography of the films were also obtained by SEM, by quenching the samples in liquid nitrogen at $T = 77\text{K}$, fracturing the film and substrate while cold, warming to room temperature, coating with Pt, and imaging (23).

The SEM images (e.g., Fig. 1C) show the smooth, curved surfaces of smectic layers terminated by distinct discontinuities, indicating that in the sublimation process, the material is removed by the nucleation coalescence and growth of holes (perhaps as small as a single molecule) in the layers, likely a process taking place on a broad range of time scales. In the presence of the TFCD array, this process is spatially modulated by the defects. Between the defects, the layers are smoothly undulated, curving down to the substrate as a TFCD center is approached. For a film initially of thickness $t > R$, where R is the TFCD radius (Fig. 2A), before any sublimation, this curvature appears as a dimpling of the surface with a conical cusp-like depression at the core of the TFCD (Fig. 2A and SI Appendix, Fig. S2). In the idealized TFCD structure, this conical depression reaches the substrate for the layer that is a distance R from the substrate at the cylinder bounding the TFCD (i.e., when the film is sublimated down to a thickness $t = R$); here, t was measured at the matrix area connecting each dimple of the TFCDs. Further sublimation would then, in principle, expose the substrate surface in a circle of radius $R = t$ about the defect center. This crossover is evident in the comparison of the layer profiles in Fig. 2A and B. In Fig. 2A, the layers are continuous, whereas in Fig. 2B, a circular region of terminated layers surrounds each TFCD core line. Thus, the YHK1 is not completely removed from the core region, and the sublimation process leaves a “dome” of layers of the TFCD. Near the center line, these layers are almost normal to the LC/air interface, an energetically costly orientation that is accommodated by the appearance of multi-Burgers vector edge dislocations at the surface, as sketched in Fig. 2. Multi-Burgers vector edge dislocations also terminate the layers at the layer steps (Fig. 1C and D).

The cross-sectional SEM view along the orange line in Fig. 1C directly reveals the internal structure of the multi-TFCD array in Fig. 1E. Within the cylindrical envelope of each TFCD (white dashes, Figs. 1E and 2A), the lower layers curve down to the substrates in circular arcs and the top smectic layers are bent toward centers of TFCDs, with a small depression at the center line of the TFCD. Fig. 1F presents a schematic model for each step during the sublimation process, and one can recognize from the evolving topography that sublimation is slower near the TFCD cores, leaving a circular dome-like structure around each TFCD center line. The number of layers that have sublimated away varies from place to place, leaving multi-Burgers vector edge dislocations, as sketched in Fig. 1D, which anneal to form smooth boundary steps on the surface topography (Fig. 1C).

Fig. 2 shows representative SEM images of a highly uniform collection of LC layers of YHK1 achieved on top of the PEI surface. SEM images and the corresponding sketches are shown for the LC film thickness; t is gradually decreasing from $5\ \mu\text{m}$ to

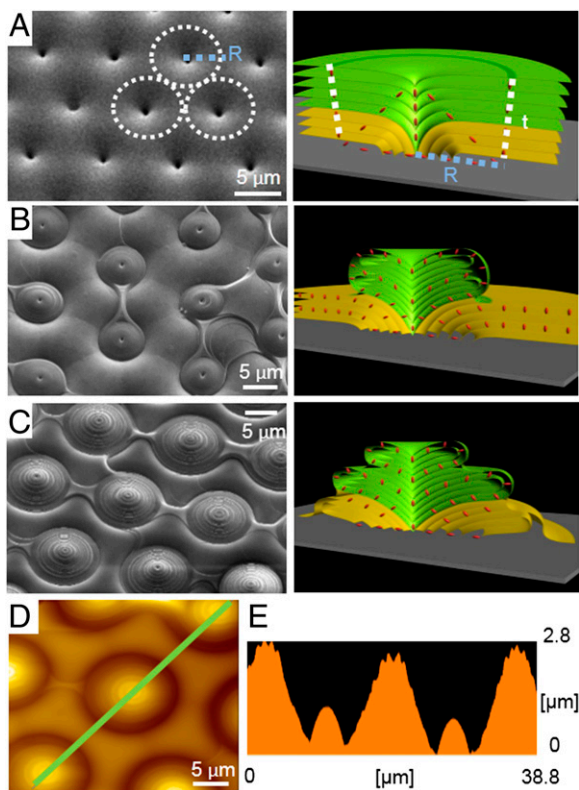


Fig. 2. Various shaped TFCDs and their schemes on the planar-aligned Si wafer as LC film thickness is changed from $5\ \mu\text{m}$ to $<2\ \mu\text{m}$ during the thermal sublimation process. (A) TFCDs ($5\ \mu\text{m} > t > \sim 3\ \mu\text{m}$), regularly formed green layers in the scheme, are the most changeable parts in the smectic film during sublimation. (B) Dome-like structures start appearing from the original dimple of premade TFCDs; here, as small depressions in the core of TFCDs at thinner films ($\sim 3\ \mu\text{m} > t > \sim 2\ \mu\text{m}$). The scheme shows how smectic layers are reformed during sublimation. (C) Concentric ring structures are easily seen in an ultrathin film condition ($\sim 2\ \mu\text{m} > t$), an interconnected area between dimples of TFCDs. (D) AFM image reveals isolated morphologies from the interconnection area between sublimated TFCDs. (E) Surface profile shows the thickness difference (200–250 nm) between terraces.

$\sim 2\ \mu\text{m}$. The radius R of $\sim 5\ \mu\text{m}$ for these TFCDs and the sublimation show that the layers are continuous and dimpled toward the substrate bottom for depths greater than R (green layers). However, the layers within a thickness t from the substrate bottom (yellow layers) bend to reach it, intersecting it at a normal incidence in the circle within R from the TFCD center line. If layers were to be simply removed to leave a film of thickness $t < R$, then the substrate bottom would be exposed within a circle of radius $R - t$ about each TFCD center. This, however, is not what is observed. Instead, under this circumstance, the circular domes about the TFCD central core lines start forming.

Effects of Surface Tension and Surface Orientational Interactions. The air/LC interface exposed by sublimation has areas where the LC surface is that of a layer and places where the layers terminate (Fig. 2). In the former case, perfect rendition of the 3D structure would have the layers parallel to the surface, whereas in the latter case, perfect rendition would have the layers normal to the surface. Typically, only one of these layer orientations is preferred, leading to some accommodation of the layering at the surface directed toward minimizing the energy of the local layer/interface interaction.

If the LC is to be removed from the surface by sublimation, in the limiting process, the air/LC interface must approach the LC/solid interface. These two interfaces have antagonistic boundary

conditions; the orientation preference has the layers normal to the solid interface and parallel to the air interface. This frustration is accommodated by the formation of multi-Burgers vector edge dislocations at the LC/air interface, enabling the layers to approach the LC/air interface normal to it but to be parallel to it immediately at the surface (green layers, Fig. 2 B and C). As sublimation proceeds and material is removed, these edge dislocation structures continuously evolve. Once the circular domes begin to form, the sublimating surface becomes inhomogeneous, presenting the flat, smooth yellow layers between the TFCDs and the edge dislocation-dominated surface of the green layers on the domes (Fig. 2 B and C). In general, these distinct regions can have different sublimation rates, and the fact that the domes persist rather than simply sublimating away down to the surface suggests that the sublimation is slower for the edge-dislocated surface. Under some circumstances, these circular domes can become much thicker than the surrounding flat layers as the sublimation proceeds (Fig. 2 D and E). As the sublimation time is extended (e.g., beyond 10 min for a $10\text{-}\mu\text{m}$ thick film), all of the LC is eventually removed.

The role of competing boundary conditions in the sublimation process was further explored by using cells with the LC in the $5\text{-}\mu\text{m}$ thick gap between clean plates (glass or silicon oxide) or between PEI-treated glass slides, all of which yield the random planar alignment (layers normal to the cell plates, as shown in the PLM image of Fig. 3 A and B) typical of fluid smectic phases. Upon cooling to room temperature, the biaxial ordering of the lower temperature phases appears as stripes parallel to the layers, enabling the layering direction in the sample plane to be visualized (Fig. 3B). Room temperature samples of this sort were cracked apart, leaving the $5\text{-}\mu\text{m}$ thick LC film exposed to air on one side and attached to a cell plate on the other. The LC/air surface was then coated with Pt as above and visualized by SEM before and after various durations of sublimation. These preparations showed clear evidence for the reorganization of the LC/air interface sketched in Fig. 4 A and B, where the surface reconstructs into the multi-Burgers vector edge dislocation structures, leaving arrays of linear bumps of near-cylindrical cross-section on the surface, with overall patterns of in-plane curvature and defects that match the PLM textures. A similar hemicylinder structure was reported by Lacaze et al. (24, 25) in the slowly cooled octylcyanobiphenyl thin film on the MoS_2 substrate, which also produces planar anchoring. These hemicylinders are shown for random planar alignment (Fig. 3 A–C) and for an in-plane aligned sample (Fig. 3 D–G, where the layer normal in the original cell is indicated by the white arrow). Thus, the frustration inherent in the competing orientation preferences at the solid and air interfaces is ameliorated by this surface transformation, which takes place in the SmA phase during the sublimation process and enables the layers to end up parallel to the LC/air interface. The energy/area, W , of the surface for the planar structure of Fig. 4A is $W = \sigma_{\parallel}$, the surface tension with the layers normal to the surface, and for the hemicylindrical structure of Fig. 4B, it is $W = \pi\sigma_{\perp}/2$, where σ_{\perp} is the surface tension with the layers parallel to the surface, and we have dropped the very small curvature elastic energy of the hemicylinders (26), $W_{\text{el}} = (\pi K/2R) \ln(R/r_c)$. The strong preference for the cylinders evident in Fig. 3 shows that σ_{\perp} must be significantly smaller than $2\sigma_{\parallel}/\pi$, and thus σ_{\perp} is the operative surface tension of the interface.

Cross-sectional images (e.g., Fig. 3G) enabled visualization of the LC/air and solid/LC surface profiles, revealing and enabling quantitative study of the curved cross-sections of the bumps. Large isolated bumps (e.g., Fig. 3F) are found to have close to a complete hemicircular cross-section, but with the circle center displaced a distance x below the surface of the solid substrate, indicating the layer structure sketched in Fig. 4C. Measurements of the ratio $r = w/h$ of the bump width, w , to height, h (SI Appendix, Figs. S3 and S4) yield a value $x/R \sim 0.15$.

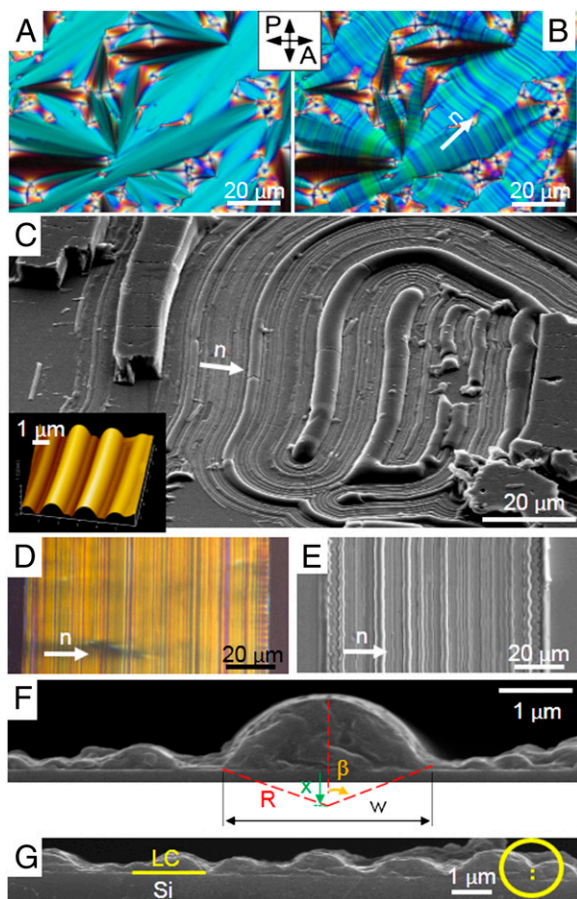


Fig. 3. Planar-aligned smectic LC before and after the thermal sublimation process. (A) PLM image from a normal planar-aligned LC shows typical fan-shaped birefringent behavior in the SmA phase. (B) Dark lines appear when the sample stays in the SmX₁ phase. (C) After removal of the coverglass and then annealing for ~2 min, sublimated morphologies appear clearly in a SEM micrograph and AFM image. (Inset) Height topography of multicylinders. The PLM image shows that the confined LC structure between the silicon rail pattern and coverglass can be aligned along the line direction (D) and also sublimated to become hemicylindrical structures (E). (F) Cross-sectional view of hemicylinders, sometimes looking like large bumps [imaginary distance x displaced below the substrate (green arrow); height h , radius R , and angle β]. (G) Small serial bumps show hemicylinders overlapped (yellow circle) together with walls.

This displacement of the circle center below the surface reduces the LC/air interface area of the surface at the expense of tilting the orientation of the layers at the solid surface away from their preferred planar orientation. Calculations (presented in *SI Appendix, Fig. S4*) show that the resulting structure depends on the ratio W_o/σ_{\perp} of the planar anchoring energy to the surface tension. For $W_o/\sigma_{\perp} \ll 1$, $x \sim R$ and the surface becomes quite flat; for $W_o/\sigma_{\perp} > 1$, $x/R \ll 1$ and the bumps become almost complete hemicylinders. The YHK1 system is in the latter regime.

In some circumstances, the hemicylinders overlap (yellow circle in Fig. 3G), giving the structure sketched in Fig. 4D. This can be understood on the basis of the competition between surface tension and the energy of grain boundary walls in the smectic layering, wherein surface energy is reduced by filling in the cusp-like depression between neighboring circular bumps, giving a cross-sectional profile such as that sketched in Fig. 4D (also calculated in *SI Appendix, Fig. S5*).

In addition to its use as a technique for nanoscale/microscale imaging, thermal sublimation is potentially useful as a soft material fabrication tool. As an example, we have explored sublimation as a process step that provides avenues for additional manipulation and control of the surface profile of microlens arrays (MLAs) templated from LC films exhibiting the spontaneous periodic ordering of TFCDs, as shown in *SI Appendix, Fig. S6* (27, 28). In polymer replicas of the self-assembled TFCD arrays, the circular focal conic defects act as positive dome-like microlenses on a nearly flat background in the interstitial region between the circular sublimated TFCDs (*SI Appendix, Fig. S6C*). However, weak sublimation induces concave curvature of the interstitial region, seen both in the SEM images of the sublimated TFCD array and its polymer replica, leading to an additional lens array producing a corresponding additional set of focused images from the replica (*SI Appendix, Fig. S6D*). These interstitial structures are clearly shown in both the SEM images of the sublimated TFCD array and its polymer replica. The focal length of this new MLA is smaller than that of the large concave MLA based on sublimated TFCDs.

Discussion

In summary, we have demonstrated that thermal sublimation can be used to show the layer structures of a smectic LC, preserving and enabling visualization of the 3D focal conic domains of the fluid SmA phase. This process restructures layer terminations at the LC/air interface into multi-Burgers vector edge dislocations that accommodate the strong preference for the smectic layers to be parallel to the air/LC surface. Additionally, we have shown that sublimation is an efficient parallel step that can be

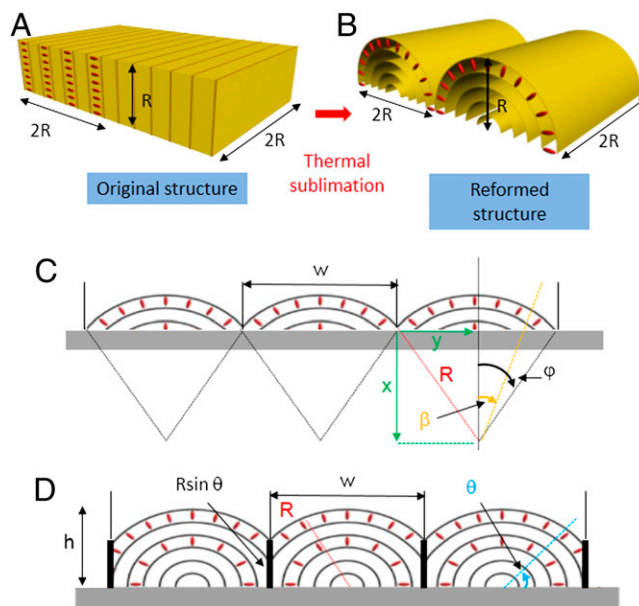


Fig. 4. Model for thermal sublimation and reformation of smectic cylinders. (A) Original planar-aligned smectic molecules between cleaned surfaces; a certain volume (of width $2R$, height R , and depth $2R$) of block is considered to determine energies forming smectic cylinders. (B) When perfect hemicylinders are formed separately, no wall exists between cylinders; planar-aligned molecules on the substrate (A) are changed to a homeotropic orientation after the thermal sublimation process. (C) If the center of hemicylinder is placed under the substrate, the scheme can be described differently, and the surface energy of an off-centered hemicylinder to the air is decreased compared with that of a perfect hemicylinder. (D) If there exist walls between cylinders, the surface area of the cylinder to the air is decreased at $(\pi - 2\theta)R^2$ and there exists a wall energy between cylinders much larger than the elastic energy of smectic cylinders.

effectively incorporated into the processing of self-assembled layered soft material systems.

It is important to emphasize that the material used, YHK1, although exhibiting a combination of properties that make it a useful demonstration material for 3D visualization by sublimation, does not possess any particularly special characteristics that should make it unique in this regard. For example, YHK1 preserves the smectic layering structure upon slow cooling to room temperature. However, it is well known that a wide variety of soft layer structures can quite generally be preserved by rapid cooling to room temperature or below; for example, there is broad application of rapid quenching in FFTEM study of LC and soft material structures. That is, appropriate combinations of cooling rate and holding temperature can preserve most soft layering structures. YHK1 is a material that thermally sublimes in the layered phase of interest at a rate that enables revelation of the internal structure in a convenient time. Sublimation rate is mostly determined by molecular size and temperature. At low temperature, for example, in FFTEM at 77K, soft matter organics, such as LCs, will not substantially thermally sublime, but the thermal sublimation of small molecular components, such as water or solvents, is commonly used in the “freeze etch” variation. However, in the circumstance where structure preservation requires low temperature, sublimation is not necessarily limited to thermal sublimation but may be assisted by ion bombardment or exposure to various etching modalities, such as sputtering or plasma etching, which, in essence, promote sublimation. It is likely that rapid quenching, observation at below room temperature, the need to supplement thermal sublimation, or various combinations of these will add complexity to the process. Nevertheless, there do exist a variety of tools available enabling the basic process demonstrated here to be broadly applied. Furthermore, there are very broad classes of organic systems developed in recent years that self-assemble in the range $250\text{ }^\circ\text{C} > T > 25\text{ }^\circ\text{C}$ to which the technique described in this paper would be directly applicable. Examples of the latter are the B7 (9) and helical nanofilament phases of bent core molecules (15). Thus, although the choice of YHK1 enables ready demon-

stration of the sublimation idea, we believe that, given the quality of structural information it develops, ways could be found to apply it broadly.

Materials and Methods

Preparation Sample and Substrate. For the sublimated TFCDs, premade normal TFCDs were annealed at slightly under isotropic temperature ($180\text{ }^\circ\text{C}$) for 2 min on the hot stage of Mettler FP82 and FP90 thermosystems. All processes were performed at the ambient condition because the sublimating rate was too fast to control in a vacuum. We investigated whether this sublimation behavior can be measured by thermogravimetric analysis experiments (SI Appendix, Figs. S7 and S8). These textures of the LC phases were monitored in situ on a polarized light microscope (Nikon LV100POL) during this process. To control the surface polarity, the glass and Si substrates were chemically cleaned by a piranha solution [$\text{H}_2\text{SO}_4/\text{H}_2\text{O}_2 = 3:1$ (vol/vol %)] to remove organic/inorganic impurities, and then repeatedly rinsed with ethanol and deionized water. To produce a tangential surface anchoring of the SmA (YHK1) at the bottom substrate, a highly uniform PEI layer (Aldrich; molecular weight of 60,000 in 1 wt% aqueous solution) 10 nm in thickness was spin-coated onto glass and silicon substrates with 5- μm deep relief to yield random planar anchoring of smectic LC.

Topographic Study. All samples for the SEM (Sirion field emission-SEM, FEI, National NanoFab Center (NNFC) at the Korea Advanced Institute of Science and Technology) were coated with a 5-nm layer of Pt to improve electron sensitivity and to protect the sample from electron beam damage. To prepare cross-sectional samples for direct examination by SEM, LC films containing various morphologies were frozen and then fractured in liquid N_2 . Topographies of sublimated LC domains were obtained using AFM (SPA400; Seiko) equipped with a 100- μm scan head. All substrates were imaged in contact mode under atmospheric conditions using standard Si_3N_4 cantilevers with a spring constant of 0.08 N/m.

ACKNOWLEDGMENTS. We thank Prof. M. C. Choi for discussions. This study was supported by grants from the National Research Foundation, funded by the Korean Government [Ministry of Science, ICT and Future Planning (MSIP)] (Grants 2012R1A1A1002486 and 2012M3A6A5054558); by the MRSEC Program, funded by National Science Foundation (NSF) Grant DMR-0820579; and by the I2CAM Junior Exchange Award, funded by NSF Grant DMR-0645461 under Institute for Complex Adaptive Matter (ICAM)-I2CAM. SEM experiments were carried out at the NNFC at the Korea Advanced Institute of Science and Technology.

- Kleman M, Lavrentovich OD (2003) *Soft Matter Physics* (Springer, New York).
- Li Z, Lavrentovich OD (1994) Surface anchoring and growth pattern of the field-driven first-order transition in a smectic-A liquid crystal. *Phys Rev Lett* 73(2):280–283.
- Lavrentovich OD, Kleman M, Pergamenschik VM (1994) Nucleation of focal conic domains in smectic A liquid crystals. *J Phys II [French]* 4(2):377–404.
- Kleman M, Lavrentovich OD (2009) Liquids with conics. *Liq Cryst* 36(10-11):1085–1099.
- Honglwan A, et al. (2013) Topographically induced hierarchical assembly and geometrical transformation of focal conic domain arrays in smectic liquid crystals. *Proc Natl Acad Sci USA* 110(1):34–39.
- Kim YH, Yoon DK, Jung HT (2009) Recent advances in the fabrication of nanotemplates from supramolecular self-organization. *J Mater Chem* 19(48):9091–9102.
- Hamley IW (1998) *The Physics of Block Copolymers* (Oxford Univ Press, Oxford).
- Bates FS, Fredrickson GH (1990) Block copolymer thermodynamics: Theory and experiment. *Annu Rev Phys Chem* 41:525–557.
- Coleman DA, et al. (2003) Polarization-modulated smectic liquid crystal phases. *Science* 301(5637):1204–1211.
- Srnalyukh II, Shiyonovskii SV, Lavrentovich OD (2001) Three-dimensional imaging of orientational order by fluorescence confocal polarizing microscopy. *Chem Phys Lett* 336(1-2):88–96.
- Choi MC, et al. (2004) Ordered patterns of liquid crystal toroidal defects by microchannel confinement. *Proc Natl Acad Sci USA* 101(50):17340–17344.
- Guo W, Herminghaus S, Bahr C (2008) Controlling smectic focal conic domains by substrate patterning. *Langmuir* 24(15):8174–8180.
- Yoon DK, et al. (2007) Internal structure visualization and lithographic use of periodic toroidal holes in liquid crystals. *Nat Mater* 6(11):866–870.
- Kim YH, et al. (2009) Confined self-assembly of toric focal conic domains (the effects of confined geometry on the feature size of toric focal conic domains). *Langmuir* 25(3):1685–1691.
- Hough LE, et al. (2009) Helical nanofilament phases. *Science* 325(5939):456–460.
- Percec V, Johansson G, Ungar G, Zhou JP (1996) Fluorophobic effect induces the self-assembly of semifluorinated tapered monodendrons containing crown ethers into supramolecular columnar dendrimers which exhibit a homeotropic hexagonal columnar liquid crystalline phase. *J Am Chem Soc* 118(41):9855–9866.
- Jeong HS, et al. (2009) Spontaneous chirality induction and enantiomer separation in liquid crystals composed of achiral rod-shaped 4-arylbenzoate esters. *J Am Chem Soc* 131(41):15055–15060.
- Prost J, Barois P (1983) Polymorphism in polar mesogens. 2. Theoretical aspects. *J Chim Phys* 80(1):65–81.
- Yoon DK, et al. (2010) Liquid-crystal periodic zigzags from geometrical and surface-anchoring-induced confinement: Origin and internal structure from mesoscopic scale to molecular level. *Phys Rev E Stat Nonlin Soft Matter Phys* 82(4 Pt 1):041705.
- Kim YH, Yoon DK, Jeong HS, Lavrentovich OD, Jung HT (2011) Smectic liquid crystal defects for self-assembling of building blocks and their lithographic applications. *Adv Funct Mater* 21(4):610–627.
- Kim YH, Yoon DK, Jeong HS, Jung HT (2010) Self-assembled periodic liquid crystal defects array for soft lithographic template. *Soft Matter* 6(7):1426–1431.
- Blanc C, Kleman M (1999) Curvature walls and focal conic domains in a lyotropic lamellar phase. *Eur Phys J B* 10(1):53–60.
- Yoon DK, et al. (2010) Organization of the polarization splay modulated smectic liquid crystal phase by topographic confinement. *Proc Natl Acad Sci USA* 107(50):21311–21315.
- Lacaze E, et al. (2004) Bistable nematic and smectic anchoring in the liquid crystal octylcyanobiphenyl (8CB) adsorbed on a MoS_2 single crystal. *Phys Rev E Stat Nonlin Soft Matter Phys* 69(4 Pt 1):041705.
- Michel JP, et al. (2004) Optical gratings formed in thin smectic films frustrated on a single crystalline substrate. *Phys Rev E Stat Nonlin Soft Matter Phys* 70(1 Pt 1):011709.
- Pishnyak OP, Nastishin YA, Lavrentovich OD (2004) Comment on “self-organized periodic photonic structure in a nonchiral liquid crystal” *Phys Rev Lett* 93(10):109401.
- Kim YH, et al. (2010) Fabrication of two-dimensional dimple and conical microlens arrays from a highly periodic toroidal-shaped liquid crystal defect array. *J Mater Chem* 20(31):6557–6561.
- Kim YH, et al. (2010) Optically selective microlens photomasks using self-assembled smectic liquid crystal defect arrays. *Adv Mater* 22(22):2416–2420.